Available online at www.sciencedirect.com
ScienceDirect
Earth and Planetary Science Letters 253 (2007) 239–253
EPSL
www.elsevier.com/locate/epsl

Seismic properties of lower crustal xenoliths from El Hoyazo (SE Spain): Experimental evidence up to partial melting

Fabio Ferri [a,*], Luigi Burlini [b], Bernardo Cesare [a,c], Raffaele Sassi [a]

[a] *Dipartimento di Mineralogia e Petrologia, Università di Padova, C.so Garibaldi 37, I-35137 Padova, Italy*
[b] *Institute of Geology, ETH Zurich, Leonhardstrasse, 19, CH-8092, Zurich, Switzerland*
[c] *C.N.R.-Istituto di Geoscienze e Georisorse, C.so Garibaldi 37, I-35137 Padova, Italy*

Received 5 May 2006; received in revised form 15 October 2006; accepted 17 October 2006
Available online 30 November 2006
Editor: R.D. van der Hilst

Abstract

Seismic techniques provide unique tools to investigate the structure and, in combination with petrological, geochemical and petrophysical study, the composition of the lower crust. Controversies can be solved with comparative study of metamorphic terrains or xenoliths that occur adjacent to areas where seismic refraction/reflection data are available. Xenoliths represent a direct sampling of the inaccessible lower crust at the time of the volcanism, whilst exposed crustal sections can only be used as analogue of present day lower crust.

The present study is focused on the measurements of compressional wave velocities up to conditions exceeding the beginning of melting (950 °C at 500 MPa confining pressure) on three garnet–biotite–sillimanite metapelitic xenoliths recovered from the Neogene dacites of El Hoyazo (SE Spain). They preserve widespread interstitial rhyolitic glass as evidence of primary melt extraction and represent the best example of partially molten lower crust in the Alborán Domain. The influence of glass on Vp is primarily reflected by anomalous positive dVp/dT while heating with velocity increasing at 500 MPa from 4.98 to 5.50 km s^{-1} at room temperature to 5.85–6.79 km s^{-1} at 650–700 °C. This corresponds to the glass transition where all the grain boundaries and most of the pores within the glass are closed. After this point, the velocity decreases to 6.2–6.5 km s^{-1} at 950 °C where re-melting of the glass is achieved and additional partial melt produced. On cooling, the behavior is normal with negative dVp/dT. After the thermal treatment velocities are 30% higher (6.07–7.21 km s^{-1}) and reveal that in the presence of intergranular melt velocity measurements at room temperature cannot be extrapolated to high temperatures.

P-waves measured at melting conditions are in agreement with deep seismic refraction data and tomography in the area and corroborate the hypothesis that partial melts are actually present in Alborán lower crust.

Keywords: seismic properties; xenolith; melting; lower crust; Petrophysics; Alborán Domain

1. Introduction

Seismic observations have provided unique tools to decipher the structure of the deep continental crust. In order to interpret the velocity profiles in terms of composition and petrology, a wide variety of experiments were performed since the pioneering works of Birch [1,2]

* Corresponding author. Tel.: +39 49 8272032; fax: +39 49 8272010.
E-mail addresses: fabio.ferri@unipd.it (F. Ferri), luigi.burlini@erdw.ethz.ch (L. Burlini), bernardo.cesare@unipd.it (B. Cesare), raffaele.sassi@unipd.it (R. Sassi).

0012-821X/$ - see front matter © 2006 Elsevier B.V. All rights reserved.
doi:10.1016/j.epsl.2006.10.027

(see [3–7]). The lower crust is directly accessible in exhumed outcrops as in Ivrea Zone and Calabria (Italy) or in xenoliths, which represent lower crustal fragments carried to surface by volcanic eruptions. Unfortunately xenolith dimensions are mostly too small for experimental investigations and large xenoliths are precious. Extremely significant are those samples which preserve traces of partial melting processes responsible for crustal differentiation. However the tentative of modelling the lower continental crust on the base of xenoliths requires some caution; in fact:

- sampling of lower crust may not be complete; most crustal xenoliths are in fact mafic and subsolidus (see [8]) while metapelitic xenoliths, and especially those with partial melt, are rare and more subject to dissolution during transport [9–11];
- because of the transport mechanisms through magmas, grain boundary modifications may occur due to rapid decompression; these involve microfracturing disaggregation of grain boundaries and melt infiltration documented by quenched glass [12,13], mineral reactions on grain boundaries and retrogressive alteration [14–16].

The presence of interstitial glass has major effects on the seismic properties of xenoliths; in mantle and crustal xenoliths measured by Parsons et al. [12], Kern et al. [13] and Gao et al. [16], for instance, samples containing glass exhibit increase of Vp with increasing temperature and anomalous low velocity with respect to similar rock types without interstitial melt and/or calculated velocities (see [14,4,6] and references therein).

This paper aims at investigating the dependence of Vp on pressure and temperature on three restitic metapelitic xenoliths recovered from El Hoyazo (south eastern Spain) up to temperatures exceeding the partial melting; the rocks are peculiar for the presence of fresh interstitial glass residue of primary melt extraction and useful to observe how anisotropy varies in concomitance with re-melting. These samples have the advantage that retrogressive reactions and other kinds of alterations related to post-melting evolution are absent except for a partial devitrification of the glass in few xenoliths.

2. Geological setting

The studied samples are xenoliths in the dacite of El Hoyazo, belonging to the Neogene Volcanic Province (hereafter NVP) of SE Spain. The NVP is a 200 km long, NE–SW trending volcanic belt at the southeastern margin of Spain [17], and consists predominantly of calc-alkaline rocks, mostly andesites [18] and minor high-K calc-alkaline to shoshonitic rocks, ranging in age from 17 to 5 Ma (references in [19–21]). The high-K calc-alkaline rocks occur as scattered, small volcanic edifices (such as El Hoyazo, see Fig. 1) and are mainly composed of Grt–Crd-bearing dacites.

Xenoliths of crustal origin are very abundant in the lavas of El Hoyazo, making up to 15% of outcrop volume [22]. The xenoliths are medium to coarse-grained granulite-facies rocks, easily recognisable by the typical presence of graphite, euhedral garnet, cordierite porphyroblasts, sillimanite and hercynitic spinel. The xenoliths have restitic bulk composition, depleted in silica and enriched in aluminium and iron (e.g. [23,24] and this paper). Xenoliths range in size from a few tens of centimetres down to single xenocrysts, which are the result of restite fragmentation and dispersion in the host lava.

Evidence of partial melting and melt extraction in the xenoliths is provided by the occurrence and high abundance of fresh rhyolitic glass (quenched melt, hereafter "glass") as primary inclusions in most minerals [23]. These S-type rhyolitic melts within the xenoliths ([25] and Acosta Vigil et al., in press) are the products of the incongruent melting of the metapelitic protoliths, not the result of melt infiltration from the enclosing dacite. In fact, the xenolith–dacite boundary is commonly sharp, without evidence of interaction. In addition, melts in inclusions and intergranular films of xenoliths are chemically different from the glass of the dacite host, which have lower Al/Si and higher K/Na [23]. Microstructures show that anatexis was accompanied by foliation development [26], indicating that the xenoliths

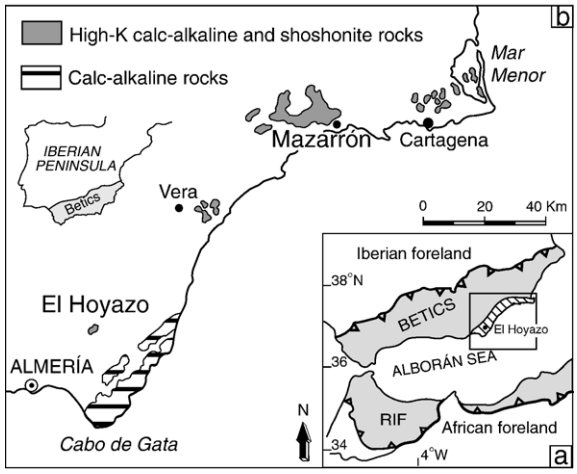

Fig. 1. Geographical location and schematic tectonic elements of the main edifices of the Miocene volcanics of the Neogene Volcanic Province within the Alborán Domain (after [55]).

represent portions of a deforming crystalline basement and were partially molten before being enclosed in the dacite.

Based on mass balances between melt inclusions, xenoliths and potential metapelitic sources, Cesare et al. [23] estimated a high degree (35–60 wt.%) of melt extraction from the xenoliths of El Hoyazo. The partial melting of the xenoliths and the development of the main assemblage (Grt–Bt–Sil–Pl–melt–Gph±Crd) have been estimated at 850±50 °C and c. 700 MPa [23]. Estimated pressures correspond to a depth of ca. 25 km (assuming a crustal density of ca. 2.7 g cm^{-3}), a value that is similar to the actual Moho depth below El Hoyazo (ca. 21 km, [27]) and that is considered to have changed very little since the end of extension in the area. Owing to the their petrographic features such as the syn-anatectic deformation [26], to their high abundance in the dacite [28], to the inferred amounts of melt extracted [23], to the estimated depth of provenance and temperatures of melting [25], the Grt–Bt–Sil xenoliths studied in this paper can confidently be considered as a proxy of the lower crust beneath the region of El Hoyazo. Such a view is supported by the persistent abundance of similar xenoliths (residual partially melted graphitic metapelites) throughout the 200-km long belt of high-K volcanics in the NVP.

Crustal melting beneath the NVP is a result of the lithospheric thinning in the Internal Betics, commenced in the early Miocene, at about 20 Ma. Although eruption of calc-alkaline crustal melts is reported for the interval 15–6 Myr [20], there are numerous indications in favour of a thermal anomaly presently active in the region: they include the very high values of surface heat flow (>80 mW m^{-2}, [29]), the anomalously thin lithosphere (<60 km, [27,30]), and the anomalously shallow, young oceanic crust in the east Alborán Sea [31]. In addition, the presence of a hot asthenospheric mantle is supported by the low velocity anomaly at shallow depth (40–60 km, [32]). More evidence for a thermal anomaly is gained from the low seismic velocity and high electrical conductivity of the lower crust [33,34], which have been interpreted as due to partially molten rocks at depth [35]. All these data suggest that melts are actually present in the lower crust from where the xenoliths have been removed.

3. Experimental techniques

3.1. Sample characterization

3.1.1. Bulk chemistry

The bulk composition of the studied xenoliths is reported in Table 1. The three compositions are remarkably similar, and similar to other analyses of Grt–Bt–Sil xenoliths from the same locality reported in the literature [22,23]. These rocks are very low in SiO_2 (45–47 wt.%) and high in Al_2O_3 (27.5–31.5 wt.%) and Fe_2O_{3tot} (11.1 wt.%). Such extreme residual character, indicative of high degrees of melt extraction, is more pronounced than in other metapelitic xenoliths of inferred restitic character, which usually have SiO_2 >50 wt.% (see summary in [4]). Another peculiar feature of the xenoliths of El Hoyazo is their high C content, reaching up to 1.2 wt.%, which explains the abundant presence of graphite in the rocks.

Table 1
Bulk composition of the xenoliths in weight %

	HO1	HO3	HO4
SiO_2	45.37	46.85	46.59
TiO_2	1.64	1.70	1.96
Al_2O_3	31.52	27.71	27.77
Fe_2O_{3tot}	11.04	11.13	11.23
MnO	0.10	0.12	0.03
MgO	2.55	2.75	3.24
CaO	1.65	2.43	2.11
Na_2O	1.98	2.66	2.70
K_2O	3.77	3.77	4.10
P_2O_5	0.19	0.27	0.13
L.O.I.[a]	1.40	1.49	2.11
Total	99.81	99.39	99.86
C	0.98	0.85	1.18
Al_2O_3/SiO_2	0.69	0.59	0.60
X_{Mg}[b]	0.31	0.33	0.36

[a] L.O.I. = Loss on Ignition.
[b] X_{Mg} = Mg/(Mg + Fetot).

3.1.2. Petrography

The samples from this study are typical Grt–Bt–Sil xenoliths from El Hoyazo [28], made of garnet, biotite, sillimanite, plagioclase, glass, graphite and minor amounts of ilmenite, cordierite or hercynite. These xenoliths have been studied in detail in previous works ([36–38] and references therein): they are medium-grained and display a well-developed foliation defined by biotite–sillimanite-rich layers and abundant graphite. The foliation often anastomoses around euhedral garnet porphyroblasts up to 8 mm in diameter and nodular aggregates of fibrolitic sillimanite intermixed with glass (hereafter called Mix), that often appear to replace garnet or other porphyroblastic phases. Plagioclase-rich domains are elongate parallel to the foliation, alternating with biotite layers. Cordierite may be present as cm-sized patchy poikiloblasts, which appear to post-date the development of the main mineral assemblage. Accessory minerals include apatite, zircon and monazite. There is often a cm-spaced mineralogical layering of Bt- Pl- or Sil-rich domains, which makes the samples quite heterogeneous at the hand-specimen scale.

The xenoliths contain abundant glass, both as an interstitial phase (e.g. in the Mix, in layer-parallel films, as coatings around garnets or pockets located at strain shadows) and as primary melt inclusions in all minerals, especially garnet and plagioclase. This indicates that all minerals crystallized in the presence of a melt phase, i.e. during partial melting. Microstructures suggest that melt was present: a) during crystallization, by incongruent melting reactions, of the main assemblage (Bt–Grt–Sil); b) during subsequent crystallization of cordierite, and c) after crystallization of restitic phases had ceased, as glass also occurs outside them as intergranular films.

3.1.3. Mineral chemistry

The mineral composition of the Grt–Bt–Sil xenoliths from El Hoyazo is very homogeneous and comparable with other analyses reported by Cesare et al. [23,36–38]. Biotite has an X_{Fe} of 0.62–0.67 and $TiO_2 \sim 5.0$ wt.%. Plagioclase is a low-Ca andesine (An_{30-33}). Garnet is weakly zoned within the ranges $Alm_{78-81}Pyp_{10-14}Sps_{1-7}Grs_{2-10}$. When present, cordierite has $X_{Fe}=0.50$. Despite slight variations among melt inclusions and interstitial glass [Acosta Vigil et al., in press], the melt is granitic, felsic and peraluminous in composition, and water-undersaturated (3–6 wt.% H_2O).

3.1.4. Geothermobarometry

Based on Grt–Bt, Grt–Crd and GASP thermobarometry, Cesare et al. [23] estimated the *P*–*T* conditions of anatexis and equilibration of the Grt–Bt–Sil xenoliths at 850±50 °C and 500–700 MPa. A further heating phase to >900 °C is recorded only in some xenoliths by the melting of biotite to hercynite+ilmenite, but this event is not observed in the studied samples.

3.1.5. Density

The grain density was measured with a helium gas pycnometer, on the same cores used for the seismic properties measurements. Before measurements, cores were desiccated for minimum 24 h at 70 °C. The bulk density was evaluated from the weight and the dimension of the cores (ρ_i in Table 2). The average grain density of the studied xenoliths is within the range 2.83–2.96 g cm^{-3} and consistent with the density of Grt–Bt–Crd–Sill gneisses and high grade metapelites reported from lower crustal sequences (e.g. [39–42]).

3.2. Seismic properties

The velocity of compressional elastic waves was measured using the pulse transmission technique [1] at temperatures up to 950 °C and pressures to 500 MPa using an internally heated gas medium apparatus (Paterson Rig). The scale sketch of the set up is reported in Fig. 2 and some additional experimental details can be found in Burlini et al. [43].

For each sample three mutually orthogonal cores (X, Y, Z) were drilled parallel to the macroscopic fabric elements: X and Y were parallel to foliation with X along the main lineation, and Z normal to foliation. The top and bottom surfaces were polished and made parallel within ±10 μm error and cores were dried at 120 °C for more than 24 h. Delay time was calibrated using a sapphire single crystal cut parallel to [0001]. The medium grain size (>1 mm) and the mineralogical layering of the xenoliths necessitate large samples to

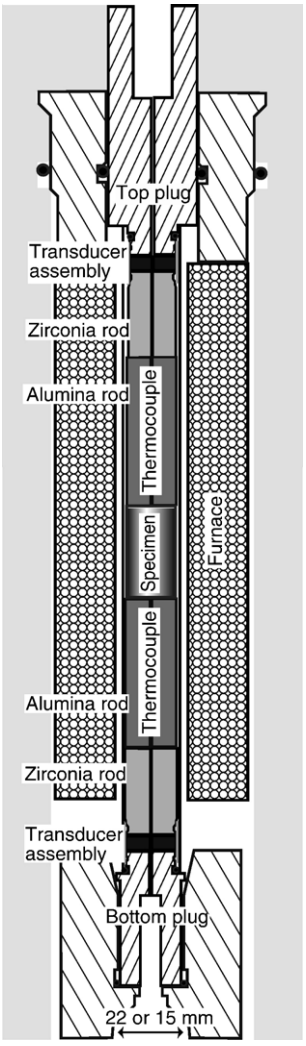

Fig. 2. Scale sketch of the experimental set up used to determine the P-wave velocities.

obtain representative measurements, so experiments were performed on cores of 22 mm diameter with about 30 mm length. Velocities were calculated as ratio between the sample length and the arrival time, measured at two frequencies (1 MHz and 0.1 MHz). Results from the two frequencies are comparable within the experimental error (±1%). Since it was not possible to exceed 700 °C using the 22 mm diameter cores, smaller cores of 15 mm diameter, cut from the same blocks in the same orientation, were used to reach the temperature of 950 °C, which is high enough to melt the interstitial glass and produce some additional partial melt (see below). On this diameter, velocities were measured on three frequencies: 3, 1 and 0.1 MHz. A part of the energy propagates as bar wave which have a lower speed than longitudinal bulk waves. For geometrical reasons (core diameter and length) the first arrival out of the noise corresponds to the P-waves only for the 0.1 and the 3 MHz, and to the bar waves for the 1 MHz. At 1 MHz, in fact, most of the longitudinal energy propagates as bar waves [1] and the arrival time of the P-waves is masked by noise. The velocities measured at 0.1 and 3 MHz coincided within the experimental error.

Temperature was measured using two R-type thermocouples (within ±1 °C) placed directly on the top and bottom sides of the sample. The difference between the two thermocouples at the highest temperature was ±5 °C. The confining pressure was measured with a manganin coil pressure transducer with a precision of about 1 MPa at 500 MPa.

The elastic wave velocities were measured with increasing confining pressure by approximately 50 MPa increments until around 500 MPa, and with decreasing confining pressure by 50 MPa decrements. After the pressure cycle, both pressure and temperature were raised at steps of 100 MPa and 100 °C until the maximum pressure and temperature were reached, then cooled down to room conditions, again by steps of about 100 °C, and finally the pressure was released by steps of about 50 MPa. The heating/cooling rate was of 3 °C/min^{-1} and measurements were performed at least 30 min after the set point was reached, to assure temperature equilibrium. Using this specific PT path we avoided thermal cracking of the samples, which were recovered intact after the tests.

The heating–cooling cycle of 15 mm cores was continuous for sample X; for Y and Z it was subdivided into steps, where samples were extracted and length/volume measured. On sample Z this was done at 600 and 650 °C, and on sample Y at 400, 600, 700 and 800 °C.

4. Results

4.1. Measurements on 22 mm diameter cores

4.1.1. Seismic properties at room temperature

The compressional wave velocity at room temperature for the 22 mm samples is reported in Fig. 3. The rod length, measured before loading, was constant during the whole compression–decompression cycle. Every sample displays the well-known initial steep increase (e.g. [2]) in compressional cycles with the velocity–pressure curves approaching linearity at pressures above 200 MPa, corresponding to closure of microcracks. Velocity hysteresis was noted in most samples during depressurization and is related to closure of cracks that

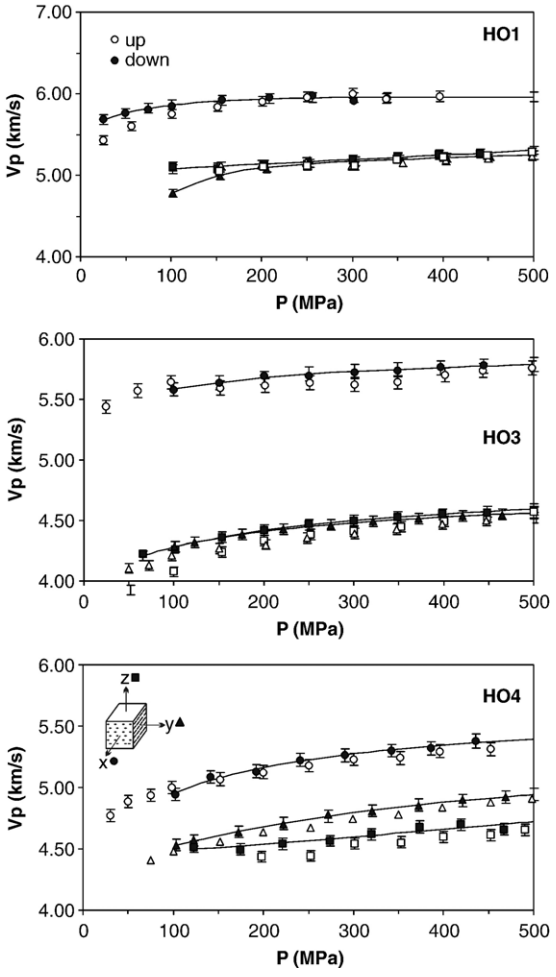

Fig. 3. Vp versus confining pressure for 22 mm diameter samples HO1, HO3 and HO4. Open symbols are measurements during pressurization and filled symbols measurements during depressurization. Circles, triangles and squares correspond to velocity measured, respectively, along X, Y and Z (see text for details).

do not reopen. In HO1 and HO3 the highest velocity is along lineation (VpX) with VpY and VpZ almost identical. This can be defined as a transverse isotropy with the axis of rotational symmetry parallel to lineation. In HO4 VpY and VpZ are similar with VpX>VpY> VpZ. This suggests a textural similarity among the xenoliths.

At 500 MPa, mean values are 5.50, 4.98 and 5.02 km s^{-1} for HO1, HO3 and HO4 respectively (see Table 2).

4.1.2. Seismic properties with moderate temperature

Samples were then heated up to ~ 700 °C at 500 MPa, and Vp revealed some peculiar features with temperature (Fig. 4). Velocity anomalously increases up to 650–700 °C; in following cooling the behavior is normal with a linear Vp increase as temperature decreases. At the same temperature, the difference in velocity before and after heating is maximum at room temperature.

At 700 °C the mean Vp (Table 2) is similar in HO1 and HO3 (6.79 km s^{-1} and 6.41 km s^{-1}) and lower in HO4 (5.85 km s^{-1}). At room temperature and 500 MPa velocity is 1.05–1.70 km s^{-1} higher after temperature treatment, corresponding to a 20–33% increment.

Heating was responsible for shortening of the rods and volume contraction producing a density increase. Since it was not possible to monitor the length decrement during the heating, the rod length was measured

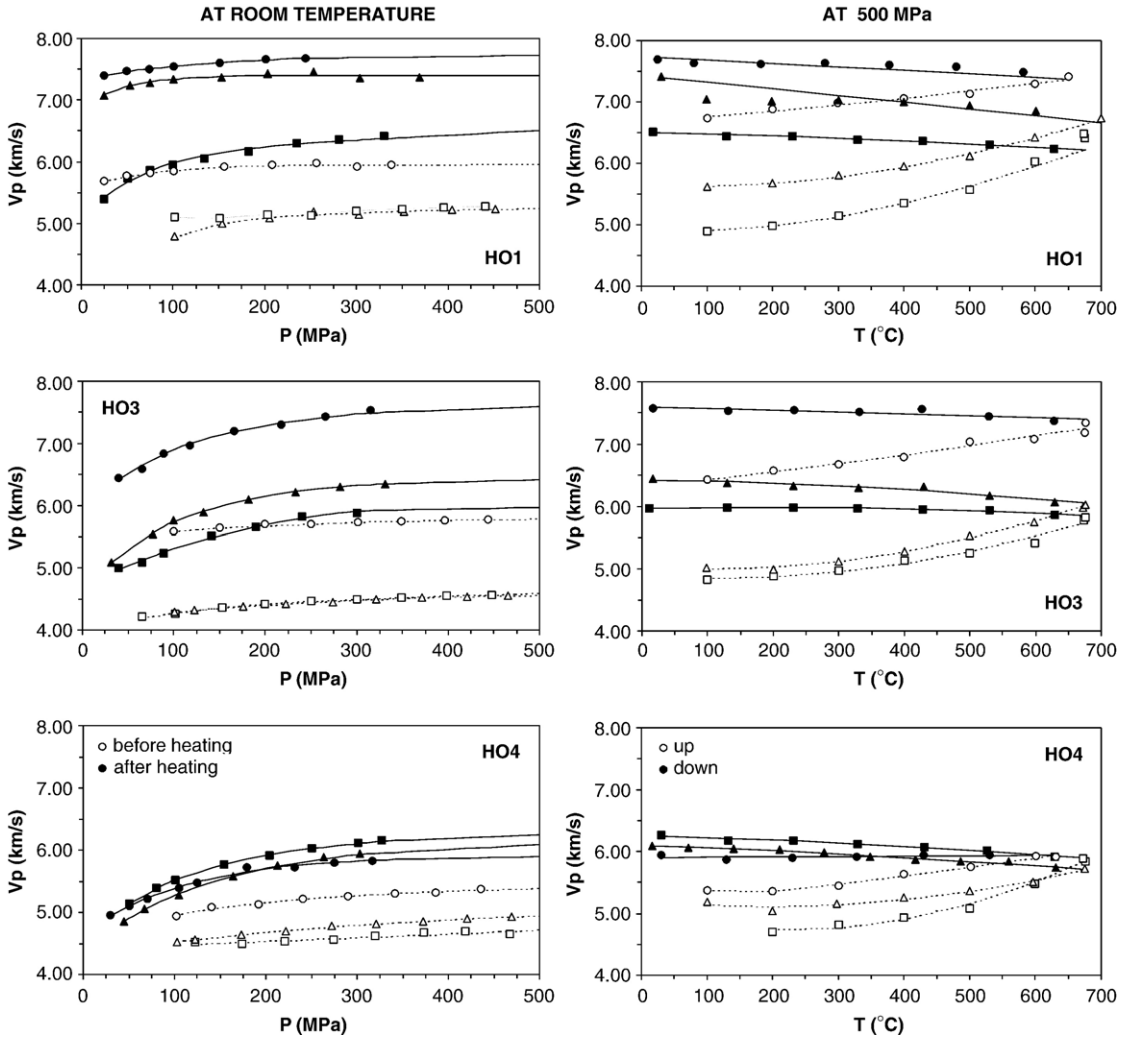

Fig. 4. Left hand side: Vp versus confining pressure at room temperature for 22 mm diameter samples. Open symbols are measurements during depressurization before heating, filled symbol measurements during depressurization after the heating–cooling cycle. Right hand side: Vp versus temperature at 500 MPa confining pressure. Open symbols are measurements during heating and filled symbols measurements during cooling. Circles, triangles and squares correspond to velocity measured, respectively, along X, Y and Z. Error smaller than symbol dimension.

before and after every run and this linear variation used to correct the velocity data. The density of the starting material ρ_i is reported in Table 2 and compared to the value measured after the run, ρ_f, on the same cylinder. ρ_p is the density of the powder determined on a different portion of the xenolith. ρ_f is always 1–2% higher than ρ_i and consistent with ρ_p except for HO1 where $\rho_p < \rho_i < \rho_f$. This low ρ_p of HO1 is attributed to high heterogeneity of the xenolith.

In Fig. 5 we plotted the Vp and the density variation at 500 MPa (dVp500 and dρ% respectively) after the heating treatment, versus the relative difference in volume dVol%. With the exception of cores HO4X and HO3X, the correlation is positive and indicates that the density and the velocity both increase as a consequence of the volume reduction (= porosity closure) and that the major the volume reduction the major the final Vp.

4.1.3. Seismic properties after temperature cycle

In Fig. 4 decompression velocity after heating (full symbols in left plots) are compared to measurements before heating (white symbols). In HO1 and HO3, VpY is higher than VpZ after heating, especially in HO1, and the original transverse isotropy (i.e. VpX > VpY = VpZ) is substituted by the relation VpX > VpY > VpZ. In HO4 the three velocities are all very similar (low anisotropy) with fastest VpZ.

The differences in velocity before and after the thermal treatments are reported in Table 2 at 500 MPa (ΔVp500) and at ambient pressure (ΔVp0) with pressure and temperature derivatives. ΔVp0 is obtained as the intercept of linear regression with zero pressure. The average ΔVp500 is similar to ΔVp0 but always slightly higher. This results in higher average pressure derivatives, within the range (3.15–5.92) 10^{-4} km s^{-1} MPa^{-1}. Such values are in agreement with the average 5.35×10^{-4} km s^{-1} MPa^{-1} proposed by Barroul and Kern [42] for metapelites.

The velocity versus temperature paths cannot be interpolated with a linear function and a more complex one is needed: $Vp = a\ e^{-T/d} + b^{T/d} + c$, where T is the absolute temperature. The coefficients are listed in Table 2.

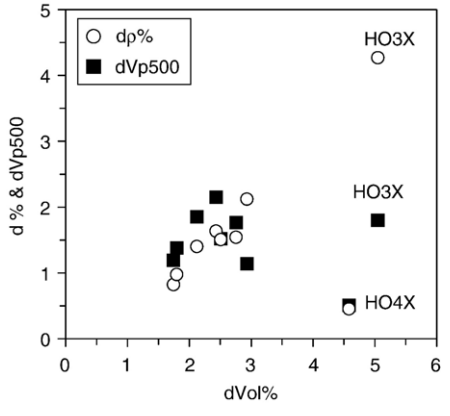

Fig. 5. The increase in velocity dVp500 and density dρ% at 500 MPa after the thermal treatment versus the relative volume reduction dVol%. Parameters defined as: $dVp500 = Vp_{final}500 - Vp_{initial}500$; $d\rho\% = 100\ (\rho_{final} - \rho_{initial})/\rho_{initial}$; $dVol\% = 100\ (Vol_{initial} - Vol_{final})/Vol_{initial}$. See text and Table 2 for details.

4.2. Measurements on 15 mm diameter cores

The sample HO1 was selected for high temperature measurements on 15 mm cylinders to reach 950 °C at 500 MPa, exceeding the T conditions estimated by Cesare et al. [23] for anatexis and equilibration of the xenoliths.

The velocities at the three different frequencies, 0.1, 1 and 3 MHz are reported in Table 3. The 3 MHz velocity are the most reliable but not always available (n.a. in the table); in fact this signal, after filtering, was never detectable before heating and never on core Z. For these intervals a comparison between 0.1 and 1 MHz data was made. The 1 MHz waves mostly propagates as bar mode [1], so that the P arrival is unreliable at high temperature, because masked by noise. At room temperature there is generally a good agreement between 0.1 and 1 MHz P wave velocity. On the basis of these observations, only the reliable data are displayed in Fig. 7.

4.2.1. Seismic properties at room temperature

Velocities at room temperature are reported in Fig. 7. Only decompression velocity is shown and behavior is linear above 150 MPa. The maximum propagation is parallel to foliation, VpX, and the minimum normal to foliation, VpZ. Comparison with velocity on 22 mm reveals similarity for VpZ, but not for VpX and VpY; these differences are attributed to the sample heterogeneity. At 500 MPa average Vp on 15-mm cores is higher than on 22 mm ones (6.24 km s^{-1} versus 5.50 km s^{-1}).

4.2.2. Seismic properties up to melting

Melting experiments were first performed on sample X which displayed a consistent length reduction–volume contraction as already observed on 22-mm cores.

In order to determine if such variation is linear, rods Y and Z were heated in steps where samples were

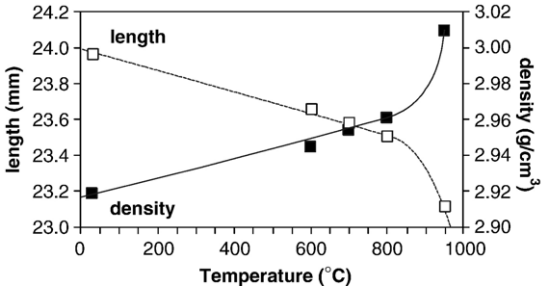

Fig. 6. Length and density variation of 15 mm diameter core Y as resulting from step heating measurements.

extracted at progressively increasing temperatures. This was done at 400 °C, 600 °C, 700 °C and 800 °C for Y, and at 600 °C and 650 °C for Z. Length, volume and density were measured after every step in sample Y while for Z only a qualitative evaluations was made. Results are plotted in Fig. 6; length linearly decreases up to 800 °C where a large decrement is registered in concomitance with melting. The density behavior is similar but with opposite sign. This length–temperature relation was used to correct the velocity data.

The results of the whole *PT* cycle are reported in Fig. 7; similarly to what observed on 22 mm cores, velocities display a positive d*V*p/d*T* on heating. In sample X, where heating was continuous up to melting, the velocity increases with temperature up to 700 °C where d*V*/d*T* becomes negative.

In sample Y the velocities measured in the first two steps (up to 400 and 600 °C) are dispersed and suggest the absence of a textural equilibrium. In the last two steps (700 and 800 °C) and during final heating up to melting, Vp regularly increased.

A different behavior was registered for sample Z where d*V*/d*T* is positive only during the first heating step to 600 °C; in subsequent coolings and heatings d*V*/d*T* is always negative. After melting a further velocity increase is registered for temperatures below 700 °C.

At 950 °C average Vp is 6.21 km s^{-1}, corresponding to ~ 10% decrement from room temperature value (6.91 km s^{-1}). The velocity reduction is particularly marked on core Z (~ 1.5 km s^{-1}) and relatively small in X and Y (0.4 and 0.2 km s^{-1} respectively).

These observations indicate that 700 °C is a crucial temperature which must be achieved to get reliable data. In particular, the transition from positive to negative d*V*/d*T* in samples X and Z suggests that at this temperature the porosity closure is almost complete. As observed on 22-mm cores, such value is close to the glass transition T_e for the intergranular rhyolitic glass [44] and has a crucial influence on glass rheology.

4.2.3. Seismic properties after melting

After the temperature cycle the average velocity is 10% higher compared to velocity before heating (Fig. 7); VpX is the highest velocity and VpY is very close to VpX (transverse isotropy). VpX and VpZ are similar to the values measured on 22-mm cores, even though mineralogy after melting is different for the growth of new phases (see below).

Pressure and temperature derivatives for 15-mm cores are reported in Table 3. At room *T* the dependence of Vp on pressure is linear (after closure of microcracks) and average d*V*/d*P* is similar to that obtained on 22-mm cores. The high temperature data were interpolated with the function: $Vp(T)=a\ e^{-T/d}+b^{T/d}+c$, where *T* is the absolute temperature.

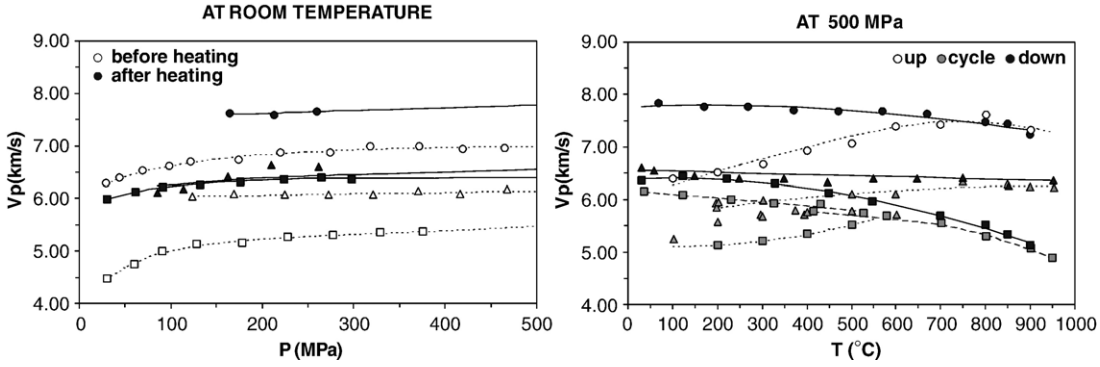

Fig. 7. Left hand side: Vp versus confining pressure at room temperature for HO1 on 15 mm diameter samples. Open symbols are Vp measured during depressurization before heating calculated from 0.1 MHz traces; filled symbols are measurements during depressurization after the heating–cooling cycle from 3 MHz traces. Right hand side: Vp versus temperature at 500 MPa confining pressure. Open symbols are measurements during heating, filled symbols measurements during cooling. VpX and VpY from 3 MHz traces, VpZ from 0.1 MHz traces. Grey symbols represent measurements for intermediate step heating (see text for details). Circles, triangles and squares correspond to velocity measured, respectively, along X, Y and Z. Error smaller than symbol dimension.

4.3. Anisotropy

One of the major aims of high temperature experiments was to observe the effects of melting on seismic anisotropy, i.e. on the directional dependence of the wave velocity. In fact melt is supposed to enhance anisotropy when its distribution is not isotropic but controlled by fabric elements such as foliation.

The intrinsic seismic anisotropy is defined as $(Vp_{max} - Vp_{min})\ 100/Vp_{mean}$ [2] and is reported in Fig. 8; for sake of simplicity, only cooling and decompression Vp are displayed. At room temperature anisotropy decreases up to 150–200 MPa which may indicate the presence of non-randomly oriented microcracks. In HO1 and HO3 anisotropy is higher than 20% while in HO4 anisotropy is much smaller (~5%).

At 500 MPa the sample HO1-15mm exhibits a remarkable increase in anisotropy with temperature, from ~ 22% at room temperature up to a maximum 35% at 950 °C. The high value is concomitant with melting and related to the strong Vp decrement affecting sample Z. This suggests that melt distribution is probably controlled by foliation but a mapping of melt location was unfortunately not possible.

In the 22 mm samples anisotropy is rather constant up to 700 °C (~ 20% in HO1, ~ 25% in HO3 and ~ 5% HO4).

5. Petrology after the temperature cycle

In the previous paragraphs we observed that velocity decreases with temperature up to 950 °C but no discontinuity in dV/dT was registered as a direct evidence for melting. The assessment of supersolidus conditions is based on the following arguments:

a) The uncorrected signals at 1 and 3 MHz evidence two major attenuation steps with temperature, one between 600 and 700 °C, and another between 900 and 950 °C. Such attenuations are probably related to the glass transition and melting temperatures (respectively the first and the second attenuation). Another minor attenuation can be envisaged at around 800 °C, where liquidus conditions for interstitial glass are achieved according to Holtz et al. [45].

b) Petrography and textures of samples after experiments were compared to starting materials (Fig. 9 a and b). At 675 °C the kinking of biotite is the only remarkable feature (Fig. 9 c and d) and no new mineral growth was observed. At 950 °C new phases are present (Fig. 9 e and f): melt (here $Melt_2$ to be distingushed from the $Melt_1$ of the starting material); Ca-enriched plagioclase (Pl_2); tiny Mg-enriched biotites (Bt_2) rimming an original large crystal of biotite (Bt_1); elongated ilmenite (Ilm) and euhedral hercynitic spinel (Spl) within glass-filled embayments in Bt_1 (Fig. 9f). This last texture is similar to that described by Cesare [25] in analogous xenoliths where it was interpreted as due to incipient melting of biotite. $Melt_2$ is abundant and concentrated in pockets or in films up to 30 μm wide, but it was not analyzed and could not be distinguished optically from $Melt_1$. Finally, widespread hematite denotes a diffuse oxidation. Since cooling after melting was not instantaneous (quench), some additional phases, like needles of biotite within melt pockets, were attributed to slow cooling.

These observations are compatible with the reaction:

$$\text{biotite}_1 + \text{plagioclase}_1 + \text{sillimanite} + \text{melt}_1 = \text{ilmenite} + \text{biotite}_2 + \text{spinel} + \text{plagioclase}_2 + \text{melt}_2$$

which is in agreement with that proposed by Cesare [25] from petrographical and chemical arguments. Cesare [25] inferred that the incongruent melting of biotite to

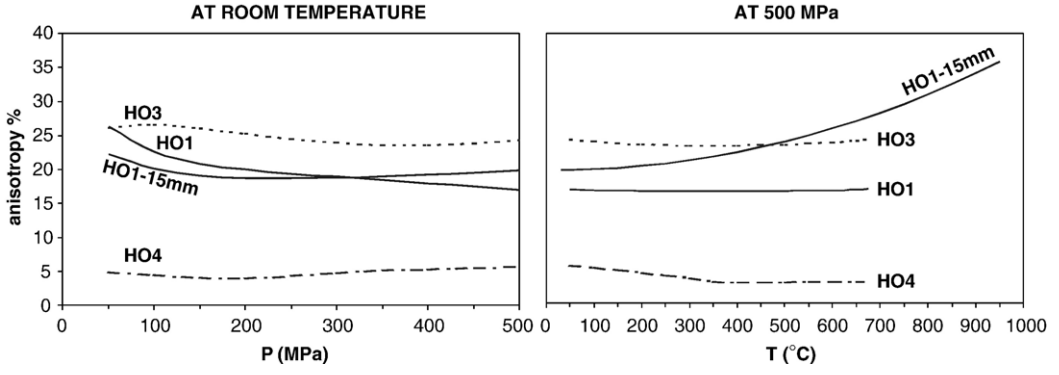

Fig. 8. Effect of confining pressure and temperature on measured seismic anisotropy $A\% = (Vp_{max} - Vp_{min})\ 100/Vp_{mean}$. Note the constant increase of anisotropy with temperature in sample HO1-15mm.

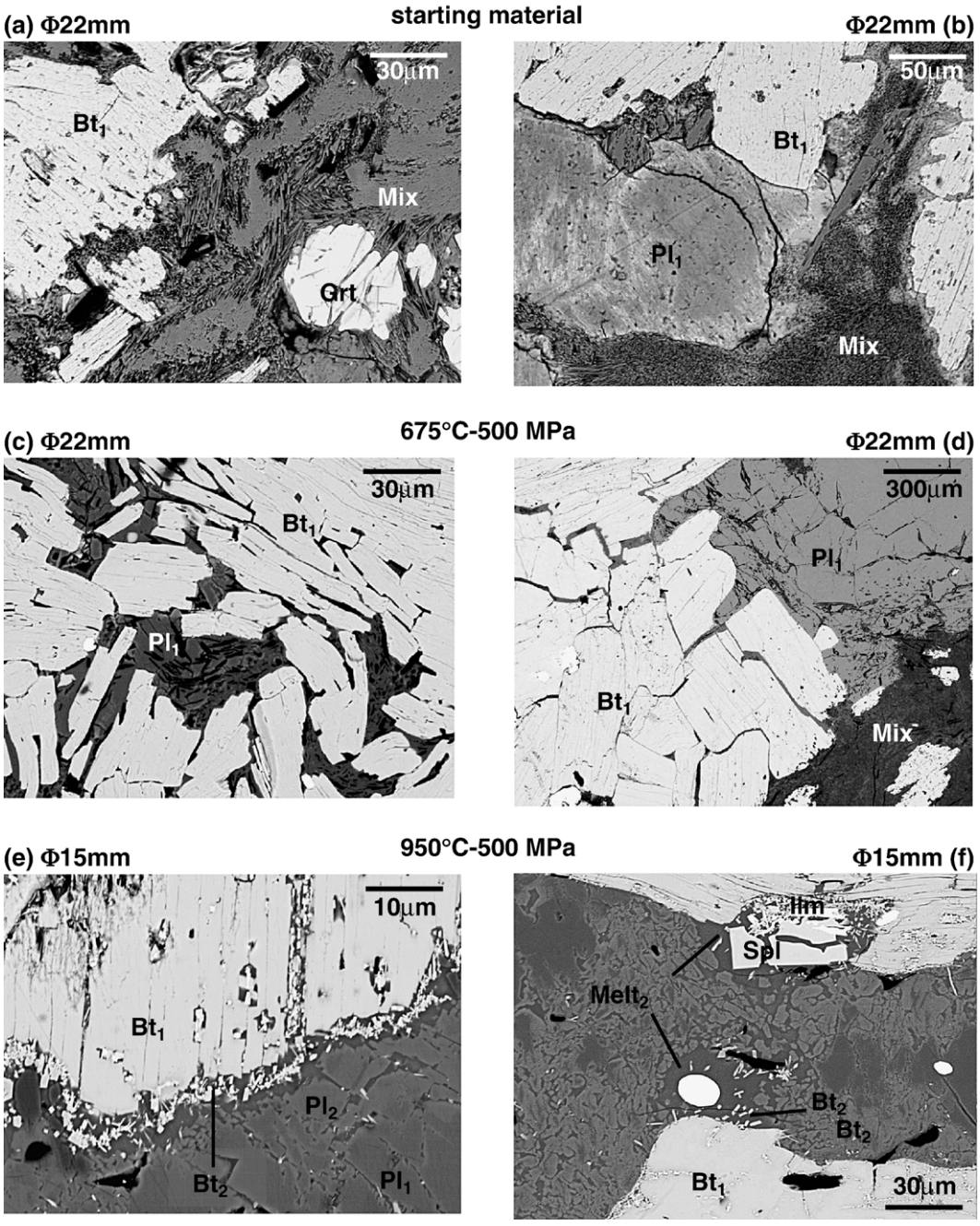

Fig. 9. Backscattered electron (BSE) images of sample HO1 (15 mm and 22 mm diameter) as a function of temperature: (a) and (b) starting material; (c) and (d) kinking of Bt_1 at 675 °C and 500 MPa; (e) and (f) growth of $Bt_2+Pl_2+Spl+Ilm$ with extensive $Melt_2$ (see text for details).

spinel at fluid-and quartz-free conditions is compatible with temperatures in the range 900–950 °C and suggested pressures around 500 MPa according to Patiño-Douce and Beard [46].

Although in the present study the reaction was not mass balanced, the coincidence of the petrographical arguments and of the pressure–temperature interval with those of Cesare [25] permits to attribute the new

Table 4
Density ρ, bulk modulus K and shear modulus G used for velocity calculation (from [47]).

	ρ	K	G
	g cm^{-3}	MPa	MPa
Sil	3.241	170.8	91.5
Grt	4.160	177.0	94.3
Pl	2.610	62.0	30.6
Bt	2.844	58.2	35.3
Gph	2.260	161.0	109.0
Ap	3.200	212.3	101.8
Zrn	4.675	227.9	109.0
Melt	2.331	37.8	30.1
Kfs	2.560	55.4	28.1

assemblage to melting, which reasonably occurred between 850 and 900 °C.

6. Measured versus calculated Vp

In order to evaluate if the measured seismic properties are consistent with the mineralogical composition, the P-waves were calculated from the volume fractions using the single crystal elastic constants and the densities reported in the compilation of Bass [47] (see list in Table 5).

The real modal composition for each rock sample was obtained using an optical microscope and a point counter. The stage feed step was set equal to the grain size of the more fine-grained sample, while the number of counted points was higher than 700 and the counter was stopped when the modal composition was not sensibly varying after incrementing the counting statistics. In Table 4 we reported the results obtained on X and Y sections from starting material together with the average of the two. In the first column of every sample, the phase "Mix" represents a fine-grained mixture of sillimanite+melt+K-feldspar [25] which cannot be resolved by optical microscopy. In order to obtain the modal proportion of these phases (second column), the average composition of the Mix was measured at the EMP (see [25] for reference analysis) and mass balanced with compositions of typical biotite and K-feldspar from El Hoyazo xenoliths (analysis reported in Cesare et al. [23,36–38]. The mass balance result (in weight %) is: Mix=66.5% sillimanite+31.7% glass+1.8% K-feldspar. These values were used to recalculate the modal proportions of every single phase, reported in the right column. A major task was to define the modal amount of melt in every sample; in Table 4 melt ranges from ~ 12% to ~ 20%. In order to assess the fidelity of such result, a Rietveld Quantitative X-Ray Diffraction (QXRD) analysis was also performed on the powdered starting material; the result is comparable with melt amounts within the range 10–15%.

Velocities were calculated using the Voigt, Reuss and Hill averaging schemes. The results are reported in Table 6. The density measured after the experiments (ρ_f in Table 6) and the intercept velocity at ambient pressure and temperature after cooling (Vp_f0 in Table 6) are in excellent agreement with those calculated with the Reuss average for HO1 and HO3 with less than 1.5% difference; for the sample HO4 the Vp difference is larger (>10%); we already observed in Fig. 5 that HO4X exhibits a low density and velocity increase after cooling despite a considerable volume reduction.

7. Discussion

The problem of fidelity between laboratory velocity and in situ conditions is of major relevance when xenoliths are investigated; transport mechanism provoke various alterations (microfracturing; disaggregation of grain boundaries; melt infiltration and vesiculation; mineral reactions and retrogressive alteration) and elastic properties are sensitive to all processes affecting microstructures. Gao et al. [16] even argued that xenoliths are not faithful samples for studying in situ seismic properties of the lower crust in terms of measured velocity unless alterations are taken into

Table 6
Comparison between calculated and measured Vp on 22 mm diameter cores

	Measured		Calculated				Differences			
	Vp^a_f0	ρ_f	Vp (V)	Vp (R)	Vp (H)	ρ	ΔV%	ΔR%	ΔH%	Δρ%
HO1	7.05	3.00	8.26	6.96	7.61	2.91	14.64	− 1.29	7.35	− 3.09
HO3	6.48	2.89	7.39	6.53	6.96	2.80	12.21	0.76	6.89	− 3.21
HO4	5.78	2.88	7.27	6.47	6.87	2.78	20.49	10.66	15.87	−3.59

[a]Symbols: Vp_f0 velocity at ambient temperature and pressure after cooling; ρ_f density after the complete pressure–temperature cycle; Vp(V), Vp(R) and Vp(H) velocity calculated with Voigt (V), Reuss (R) and Hill (H) averaging schemes respectively; ρ calculated density; ΔV%, ΔR% and ΔH% percentage difference between calculated and measured velocities using the three different averaging schemes.

account. In the presence of glass, cognate or infiltrated from host lavas, discrepancies are mostly attributed to the additional porosity induced by volume contraction and/or vesiculation of the cooled glass. The major effects are: (a) room temperature Vp lower than those measured on analogue rock types from exposed crustal sequences [12]; (b) anomalously positive dVp/dT [13,16].

Both the anomalies are observable in our measurements (Figs. 3 and 4):

a) During the room temperature decompression preceding the thermal treatment velocity is 4.98–5.50 km s^{-1}, lower than in comparable high grade metasediments. Samples from exposed crustal sections as stonalites and kinzigites from the Ivrea Zone (Northern Italy) or paragranulites from Calabria (Southern Italy) give 6.50–7.55 km s^{-1} [40] and 6.75 km s^{-1} [39] respectively, in agreement with the averaged 6.5–7.0 km s^{-1} proposed by Rudnick and Fountain [4] for deep crustal levels. After the thermal treatment Vp increases to 6.07–7.21 km s^{-1} which are compatible with the average lower crustal data.
b) A positive dVp/dT is observed during the heating up to 650–700 °C which corresponds to the interval where the glass transition T_e for rhyolitic glasses occurs [44]. The velocity increases with temperature till all the pores within the glass and on the grain boundaries are closed as demonstrated by the general volume contraction and density increase. After that, the velocity can start to decrease. Up to about 800 °C we only reached that point when the melt has gone through the glass transition and was liquid again, in agreement with Holtz et al. [45]. The petrographical analysis demonstrates that growth of new mineral concomitant with melting occurs only between 850 and 950 °C where the velocities are remarkably high (~ 6.2 km s^{-1} in sample HO1). During the cooling and decompression the excess porosity of the starting material is not recovered. In fact when the cooling occurs at high pressure:
   – the gas solubility in the melt is higher and the melt vesiculation is reduced [45];
   – part of the free volume eventually produced during the contraction of the glassy material is compensated by the external overpressure.

From our experiments we can drive some remarks:

i) the temperature required to eliminate most of the effects of porosity is above the glass transition; since this temperature is actually an interval rather than a single value, we suggest to perform measurements up to 650 °C in presence of rhyolitic intergranular glass [44] and 750 °C for basaltic ones ([48] and references therein);
ii) the volume variation must be monitored during the experiment, to correct the velocity measurements for the length change.

The effect of the presence of melt on the seismic velocity is large but not well constrained by either experimental or theoretical results. Though the variation in elastic properties between melt and rocks is considerable (V_p melt ≈ 3 km s^{-1}; V_p rock ≈ 7 km s^{-1}) the major uncertainty is due to the strong dependence on melt geometry especially when a connecting network of melt is achieved.

Since the work of Murase and Kushiro [49] on a dry spinel lherzolite, it was verified that the onset of melting is reflected by a systematic Vp decrement with increasing degree of partial melting. The velocity does not markedly change at the solidus temperature but decreases substantially once the amount of partial melt exceeds about 2%. When the melt percentage is about 20% Vp reduction is ~ 30%. A similar behavior is confirmed by the melting of amphibolitic rocks [50] and granites [50,51] though the superposition of parallel processes like thermal cracking, dehydration or phase transitions introduces some complexities. In the granite studied by Mueller and Massonne [51] dVp/dT changes from -2.43×10^{-4} km s^{-1} °C^{-1} within the interval 20–400 °C to -6.42×10^{-3} km s^{-1} °C^{-1} for the range 900–1200 °C where 40% of melt is observed. Similarly in the amphibolite investigated by Aizawa et al. [50] the temperature coefficient passes from -5.4×10^{-4} km s^{-1} °C^{-1} below the solidus to -5.0×10^{-3} km s^{-1} °C^{-1} at 800 °C where the amount of melt is around 20%.

In Fig. 7 the velocity decreases linearly with temperature above ~ 700 °C and dVp/dT is constant up to 950 °C; the production of further melt between 850 and 950 °C doesn't affect the temperature derivatives. This different behavior with respect to [49–51] can be explained if we consider that our xenoliths originally contained 10–15% of interstitial glass which dominates the temperature dependency of seismic properties. Between the glass transition (~ 700 °C) and the liquidus temperature (~ 800 °C) the total amount of glass becomes suddenly fluid and presumably interconnected so that the transitions from subsolidus to beginning of melting and then to extensive melting are not visible.

For directions Y and Z the dVp/dT coefficients at temperature > Tg are similar, -2.1×10^{-4} for Y and -2.0×10^{-3} km s^{-1} °C^{-1}; for X it is -1.2×10^{-3} km s^{-1} °C^{-1}.

These values are all comparable with those reported by Murase and Kushiro [49] and Mueller and Massonne [51] for the interconnected melt pathways.

The average velocity corrected to 950 °C at 500 MPa for samples HO3 and HO4 are 6.38 and 6.17 km s^{-1}; the average Vp for HO1 reported to 950 °C for the 22-mm cores is 6.51 km s^{-1} which is 5% higher than the measurement on the 15-mm cylinders (6.21 km s^{-1}). The data on single directions evidence that consistency is good for directions X (7.21 versus 7.25 km s^{-1}) and Y (6.39 versus 6.36 km s^{-1}) but differences are substantial on Z core (5.92 versus 5.03 km s^{-1}). This is attributed either to melt redistribution after melting affecting the sample anisotropy or to compositional differences of the starting materials (e.g. amount of glass).

All these considerations suggest that the most realistic values for Vp in the lower crust beneath the Betic/Alborán Domain, if a partially molten material is assumed, are in the range 6.2–6.5 km s^{-1}.

Deep seismic refraction data [52,53] and tomographies [33] from middle and lower crust in SE Spain revealed that the area is characterized by low average compressional velocity in the range 6.3–6.5 km s^{-1} from 10 km depth down to 22 km which corresponds to the actual position of the Moho in the area [54]. Cesare et al. [23] showed that graphitic metapelites from nearby Alpujarride basement of Betic Cordillera can be considered the potential protoliths for El Hoyazo xenoliths and Zappone et al. [35] determined the compressional velocity of these rocks up to 280 MPa; laboratory Vp are in the range 6.45–6.94 km s^{-1}. The combination of the veloctiy from Zappone et al. [35] for the middle crust with our experimental results for the lower crust delineate a seismically homogeneous crust section from 10 km down to the Moho, which is in agreement with field data by Carbonell et al. [33]. In this view, the field seismic profiles combined with the laboratory measurements support the hypothesis that the Alborán lower crust is mostly composed of metasediments which are partially molten at the deepest level.

8. Conclusions

- We measured the seismic properties of metapelitic xenoliths up to 950 °C at 500 MPa. We observed that during the temperature increment the velocities increased instead of decreasing up to 650–700 °C, corresponding to the glass transition, but decreased at higher temperatures (e.g. from 5.34 km s^{-1} at 400 °C to 5.69 km s^{-1} at 650 °C and 4.90 km s^{-1} at 950 °C). This corresponded to ~ 3% reduction of the volume from room temperature to 950 °C due to reorganization of the glass inside the sample and leads to the pore reduction. During cooling the velocities increased from 4.90 km s^{-1} at 900 °C to 6.40 km s^{-1} at room conditions. This hysteresis loop was caused by the porosity produced during the uprise of the xenoliths for rapid cooling and decompression.
- From the above observation we recommend to measure seismic properties of xenoliths at concomitant high pressure–high temperature above the glass transition.
- The seismic anisotropy remarkably increased with temperature up to a maximum 35% after melting which suggests a control of the fabric on melt distribution.
- At melting, the average Vp was 6.2–6.5 km s^{-1} which is remarkably higher than values expected for supersolidus conditions. This velocity is in agreement with the seismic profiles in the area and supports the hypothesis of the actual presence of partial melts in the Alborán lower crust.

Acknowledgements

This work has been made possible thanks to the support of the University of Padova (Assegni di Ricerca 2003) and of the 01-LECEMA22F "WESTMED—Imaging the western Mediterranean margins: a key target to understand the interaction between deep and shallow processes" Project by the European Science Foundation under the EUROCORES Programme EUROMARGINS, through contract No. ERAS-CT-2003-980409 of the European Commission, DG Research, FP6." R. Hofmann and M. Mettler are gratefully thanked for the technical assistance at ETH (Zurich), M. T. Gómez-Pugnaire (Universidad de Granada) for field-work assistance, and M. Dapiaggi (Università Statale di Milano) for Rietveld refinements. The experiments were performed in the Experimental deformation laboratory of Zurich with the equipment installed with the support of the NF R'Equip project #2160-053289.98 and ETH Berufungskredit (ETH # 0-42073-93/3392) of Prof. J.-P. Burg. Constructive reviews by Frank Schilling are greatly appreciated.

Appendix A. Supplementary data

Supplementary data associated with this article can be found, in the online version, at doi:10.1016/j.epsl.2006.10.027.

References

[1] A.F. Birch, The velocity of compressional waves in rocks to 10 kilobars, Part 1, J. Geophys. Res. 65 (1960) 1083–1102.
[2] A.F. Birch, The velocity of compressional waves in rocks to 10 kilobars, Part 2, J. Geophys. Res. 66 (1961) 2199–2224.

[3] W.S. Holbrook, W.D. Mooney, N.I. Christensen, The seismic velocity structure of the deep continental crust, in: D.M. Fountain, R. Arculus, R.W. Kay (Eds.), Continental Lower Crust, Developments in Geotectonics, vol. 23, Elsevier, Amsterdam, 1992, pp. 1–43.
[4] R.L. Rudnik, D.M. Fountain, Nature and composition of the continental crust: a lower crustal perspective, Rev. Geophys. 33 (1995) 267–309.
[5] N.I. Christensen, W.D. Mooney, Seismic velocity structure and composition of the continental crust: a global view, J. Geophys. Res. 100 (1995) 9761–9788.
[6] T. Weiss, S. Siegesmund, W. Rabbel, T. Bohlen, M. Pohl, Seismic velocity and anisotropy of the lower continental crust: a review, Pure Appl. Geophys. 156 (1999) 97–122.
[7] R.L. Rudnick, S. Gao, The Composition of the Continental Crust, in: R.L. Rudnick (Ed.), The Crust, Treatise on Geochemistry vol. 3 (H.D. Holland and K.K. Turekian Eds.), Elsevier–Pergamon, Oxford, 2003, pp. 1–64.
[8] R.L. Rudnick, Xenoliths — samples of the lower continental crust, in: D.M. Fountain, R. Arculus, R.W. Kay (Eds.), Continental Lower Crust, Developments in Geotectonics, vol. 23, Elsevier, Amsterdam, 1992, pp. 269–316.
[9] A. Tsuchiyama, Melting and dissolution kinetics: application to partial melting and dissolution of xenoliths, J. Geophys. Res. 91 (1986) 9395–9406.
[10] P.M. Sachs, S. Stange, Fast assimilation of xenoliths in magmas, J. Geophys. Res. 98 (1993) 19,741–19,754.
[11] P. McLeod, R.S.J. Sparks, The dynamics of xenolith assimilation, Contrib. Mineral Petrol. 132 (1998) 21–33.
[12] T. Parsons, N.I. Christensen, H.G. Wilshire, Velocities of southern Basin and Range xenoliths: insights on the nature of lower crustal reflectivity and composition, Geology 23 (1995) 129–132.
[13] H. Kern, L. Burlini, I.V. Ashchepkov, Fabric-related seismic anisotropy in upper-mantle xenoliths: evidence from measurements and calculations, Phys. Earth Planet. Inter. 95 (1996) 195–209.
[14] I. Jackson, R.L. Rudnick, S.Y. O'Reilly, C. Bezant, Measured and calculated elastic wave velocities for xenoliths from the lower crust and upper mantle, Tectonophysics 173 (1990) 207–210.
[15] R.L. Rudnick, I. Jackson, Measured and calculated elastic wave speed in partially equilibrated mafic granulite xenoliths: implications for the properties of an underplated lower continental crust, J. Geophys. Res. 100 (1995) 10,211–10,218.
[16] S. Gao, H. Kern, Y.S. Liu, S.Y. Jin, T. Popp, Z.M. Jin, M. Sun, Z.B. Zhao, Measured and calculated seismic velocities and densities for granulites from xenoliths occurrences and adjacent exposed lower crustal sections: a comparative study from the North China craton, J. Geophys. Res. 105 (2000) 18965–18976.
[17] J. López-Ruiz, J. Cebriá, M. Doblas, Cenozoic volcanism I: the Iberian Peninsula, in: W. Gibbons, T. Moreno (Eds.), The Geology of Spain, Geol. Soc. London, UK, 1980, pp. 417–438.
[18] J.M. Fernández-Soler, El volcanismo calco-alcalino en el parque natural de Cabo de Gata-Níjar (Almería). Estudio Volcanológico Y Petrológico, PhD thesis, Sociedad Almeriense de Historia Natural, Monografías del Medio Natural 2, 1996.
[19] H.P. Zeck, A.B. Kristensen, I.S. Williams, Post-collisional volcanism in a sinking slab setting— crustal anatectic origin of pyroxene–andesite magma, Caldear Volcanic Group, Neogen Alborán volcanic Province, south-eastern Spain, Lithos 45 (1998) 499–522.
[20] S.P. Turner, J.P. Platt, R.M.M. George, S.P. Kelley, D.G. Pearson, G.M. Nowell, Magmatism associated with orogenic collapse of the Betic–Alborán Domain, SE Spain, J. Petrol. 40 (1999) 1011–1036.
[21] S. Duggen, K. Hoernle, P. Van Den Bogaard, C. Harris, Magmatic evolution of the Alborán region: the role of subduction in forming the western Mediterranean and causing the Messinian salinity crisis, Earth Planet. Sci. Lett. 218 (2004) 91–108.
[22] H.P. Zeck, Anatectic origin and further petrogenesis of almandine-bearing biotite–cordierite–labradorite dacite with many inclusions of restite and basaltoid material, Cerro de Hoyazo, SE Spain, PhD thesis, Amsterdam, The Netherlands, 1968.
[23] B. Cesare, E. Salvioli Mairani, G. Venturelli, Crustal anatexis and melt extraction during deformation in the restitic xenoliths at El Joyazo (SE Spain), Min. Mag. 61 (1997) 15–27.
[24] R. Benito, J. López-Ruiz, J. Cebriá, Sr and O isotope constraints on source and crustal contamination in the high-K calc-alkaline and shoshonitic Neogene volcanic rocks of SE Spain, Lithos 46 (1999) 773–802.
[25] B. Cesare, Incongruent melting of biotite to spinel in a quartz-free restite at El Joyazo (SE Spain): textures and reaction characterization, Contrib. Mineral Petrol. 139 (2000) 273–284.
[26] B. Cesare, M.T. Gomez-Pugnaire, Crustal melting in the Alborán domain: constraints from the xenoliths of the Neogene Volcanic Province, Phys. Chem. Earth 26 (2001) 255–260.
[27] M. Torne, M. Fernández, M.C. Comas, J.I. Soto, Lithospheric structure beneath the Alborán Basin; results from 3-D gravity modeling and tectonic relevance, J. Geophys. Res. 105 (2000) 3209–3228.
[28] H.P. Zeck, An erupted migmatite from Cerro de Hoyazo, SE Spain, Contrib. Mineral. Petrol. 26 (1970) 225–246.
[29] M. Fernández, I. Marzán, A. Correia, E. Ramalho, Heat flow, heat production and lithospheric thermal regime in the Iberian Peninsula, Tectonophysics 191 (1998) 29–53.
[30] W. Spakman, R. Wortel, A tomographic view on Western Mediterranean geodynamics, in: W. Cavazza, F. Roure, W. Spakman, G.M. Stampfli, P.A. Ziegler (Eds.), The TRANSMED Atlas, The Mediterranean Region from Crust to Mantle, Springer, Berlin Heidelberg, 2004, pp. 31–52.
[31] B.G. Polyak, M. Fernández, M.D. Khutorskoy, J.J. Soto, I.A. Basov, M.C. Comas, V.Y. Khain, B. Alonso, G.V. Agapova, I.S. Mazurova, A. Negredo, V.O. Tochitsky, N.A. Bogdanov, E. Banda, Heat flow in the Alborán Sea (the western Mediterranean), Tectonophysics 263 (1996) 191–218.
[32] A. Calvert, E. Sandvol, D. Seber, M. Baranzagi, S. Roecker, T. Mourabit, F. Vidal, G. Alguacil, N. Jabour, Geodynamics evolution of the lithosphere and upper mantle beneath the Alborán region of the western Mediterranean: constraints from travel time tomography, J. Geophys. Res. 105 (2000) 10871–10898.
[33] R. Carbonell, V. Sallarés, J. Puos, J.J. Dañobeitia, P. Queralt, J.J. Ledo, G. Dueñas, A multidisciplinary geophysical study in the Betic chain (southern Iberia Peninsula), Tectonophysics 288 (1998) 137–152.
[34] J. Pous, P. Queralt, J. Ledo, E. Roca, A high electrical conductive zone at lower crustal depth beneath the Betic Chain (Spain), Earth Planet. Sci. Lett. 167 (1999) 35–45.
[35] A. Zappone, M. Fernàndez, V. Garcia-Duenas, L. Burlini, Laboratory measurements of seismic P-wave velocity on rocks from the Betic chain (southern Iberian Peninsula), Tectonophysics 317 (2004) 259–272.
[36] B. Cesare, G. Cruciani, U. Russo, Hydrogen deficiency in Ti-rich biotite from anatectic metapelites (El Joyazo– SE Spain):

crystal–chemical aspects and implications for high-temperature petrogenesis, Am. Mineral. 88 (2003) 583–595.
[37] B. Cesare, C. Marchesi, J. Hermann, M.T. Gomez-Pugnaire, Primary melt inclusions in andalusite from anatectic graphitic metapelites: implications for the position of the Al_2SiO_5 triple point, Geology 31 (2003) 573–576.
[38] B. Cesare, S. Meli, L. Nodari, U. Russo, Fe^{3+} reduction during biotite melting in graphitic metapelites: another origin of CO_2 in granulites, Contrib. Mineral. Petrol. 149 (2005) 129–140.
[39] H. Kern, V. Schenk, A model of the velocity structure beneath Calabria, southern Italy, based on laboratory data, Earth Planet. Sci. Lett. 87 (1988) 325–337.
[40] M.M. Burke, D.M. Fountain, Seismic properties of rocks from an exposure of extended continental crust— new laboratory measurements from Ivrea Zone, Tectonophysics 182 (1990) 119–146.
[41] G. Barruol, D. Mainprice, 3D seismic velocities calculated from lattice-preferred orientation and reflectivity of a lower crustal section: examples of the Val Sesia section (Ivrea zone, northern Italy), Geophys. J. Int. 115 (1993) 1169–1188.
[42] G. Barruol, H. Kern, Seismic anisotropy and shear-wave splitting in lower-crustal and upper-mantle rocks from Ivrea zone— experimental and calculated data, Phys. Earth Planet. Inter. 95 (1996) 175–194.
[43] L. Burlini, L. Arbaret, G. Zeilinger, J.P. Burg, High-temperature and pressure seismic properties of a lower crustal prograde shear zone from the Kohistan Arc Pakistan, in: D. Bruhn, L. Burlini (Eds.), High-Strain Zones: Structure and Physical Properties, Geol. Soc. Spec. Public., vol. 245, 2005, pp. 187–202.
[44] D.B. Dingwell, The glass transition in hydrous granitic melts, Phys. Earth Planet. Inter. 107 (1998) 1–8.
[45] F. Holtz, W. Johannes, N. Tamic, H. Behrens, Maximum and minimum water contents of granitic melts generated in the crust: a reevaluation and implications, Lithos 56 (2001) 1–14.
[46] A.E. Patiño-Douce, J.S. Beard, Effects of P, $f(O_2)$ and Mg/Fe ratio on dehydration melting of model metagreywackes, J. Petrol. 37 (1996) 999–1024.
[47] J.D. Bass, Elasticity on minerals, glasses and melts, in: T.J. Ahrens (Ed.), Mineral Physics and Crystallography. A handbook of Physical Constants, AGU Reference Shelf, vol. 2, 1995, pp. 45–63.
[48] F.R. Schilling, S.V. Sinogeikin, M. Hauser, J.D. Bass, Elastic properties of model basaltic melt compositions at high temperatures, J. Geophys. Res. 108 (2003) 2304.
[49] T. Murase, I. Kushiro, Compressional wave velocity in partially molten peridotite at high pressures, Year B. – Carnegie Inst. Wash. 78 (1979) 559–562.
[50] Y. Aizawa, K. Ito, Y. Tatsumi, Compressional wave velocity of granite and amphibolite up to melting temperatures at 1 GPa, Tectonophysics 351 (2002) 255–261.
[51] H.J. Mueller, H.J. Massonne, Experimental high pressure investigation of partial melting in natural rocks and their influence on Vp and Vs, Phys. Chem. Earth 26 (2001) 325–332.
[52] E. Banda, J. Gallart, V. Garcia-Dueñas, J.J. Dañobeitia, J. Makris, Lateral variation of the crust in the Iberian peninsula: new evidence from the Betic Cordillera, Tectonophysics 221 (1993) 53–66.
[53] J. Julià, F. Mancilla, J. Morales, Seismic signature of intracrustal magmatic intrusions in the Eastern Betics (Internal Zone), SE Iberia, Geophys. Res. Lett. 32 (2005) L16304.
[54] M.C. Comas, J.P. Platt, J.I. Soto, A.B. Watts, The origin and tectonic history of the Alborán basin: insights from leg 161 results, in: R. Zahn, M.H. Comas, A. Klaus (Eds.), Proc. ODP, Scientific Results, vol. 161, 1999, pp. 555–579.
[55] J. López-Ruiz, E. Rodríguez Badiola, La region volcanica Neogena del sureste de España, Estud. Geol. 36 (1980) 5–63.